

Gaële Perret, Marie Farge, Alexandre Stegner, Alexandre Azzalini
Laboratoire de Météorologie Dynamique, ENS, Paris
and Kai Schneider
Laboratoire de Modélisation et de Simulation Numérique, CNRS, Marseille

ABSTRACT: We present a new numerical method to compute the rotating shallow water equations past a cylindrical obstacle which is impulsively started. It combines a pseudo-spectral scheme and a volume penalization method to take into account the no-slip boundary conditions on the obstacle. We present here several experiments to study the effect of rotation on the von Karman street which develops in the wake of the obstacle. In order to check the numerical results, we also perform several laboratory experiments using a two-layer stratified flow on a turn-table where a cylindrical obstacle is translated. We qualitatively compare the vorticity fields obtained by particle image velocimetry (PIV) with those computed by the numerical experiments for the same set of parameters.

1 INTRODUCTION

In contrast to the incompressible two-dimensional von Karman street, wakes encountered in geophysical flows are affected by the Earth's rotation and the vertical stratification. We use the rotating shallow-water model as the simplest model to account for the influence of the Coriolis force and allow divergent motions.

Previous studies have shown that an asymmetry could occur between vortices of opposite signs when the characteristic scale is larger than the Rossby deformation radius, the scale above which the effect of the Earth's rotation becomes significant. Numerical simulations of decaying shallow water turbulence have shown significant differences in shape and strength between cyclonic and anticyclonic vortices (Farge and Sadourny 1989; Polvani et al. 1994). Namely, at scales larger than the Rossby deformation radius, anticyclones tend to be more circular and less distorted than their cyclonic counterparts. Moreover, the same cyclonic-anticyclonic asymmetry has also been observed in other rotating shallow water flows for isolated vortices (Stegner and Dritschel 2000) and jets (Poulin and Flierl 2003). Such effect can also be observed in the ocean in the wake of islands whose size is larger than the Rossby deformation radius (Figure 1).

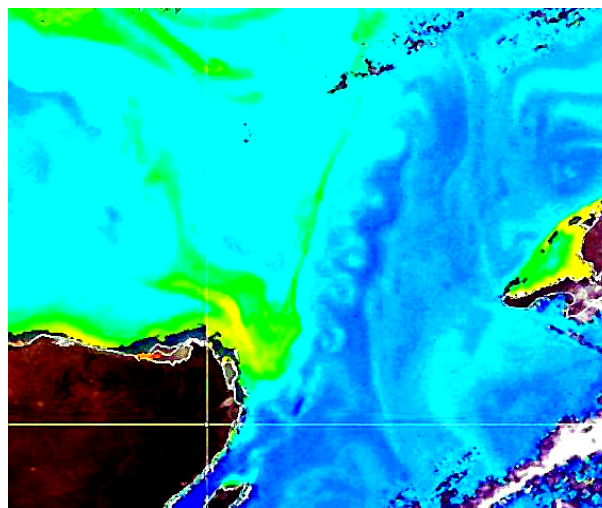


Figure 1. Oceanic wake past Isla Mujeres, an island off the peninsula of Yucatan (Mexico). The color corresponds to the phytoplankton concentration which is passively advected by the flow. We observe that the anticyclonic vortices are quasi-circular while the cyclones are elongated.

The numerical experiments presented in this paper are based on a new method which combines a pseudo-spectral scheme with a volume penalization to take into account the presence of an obstacle in the flow. It has already been used to compute a two-dimensional incompressible flow past an impulsively started cylinder (Schneider and Farge 2002). We extend this method to the case of two-dimensional compressible flows in the context of the shallow water approximation. The laboratory experiments are performed with a two-layers stratified flow and the obstacle is translated in the upper layer only, while the bottom layer remains almost at rest in the rotating frame.

2 MODEL

2.1 Theoretical model

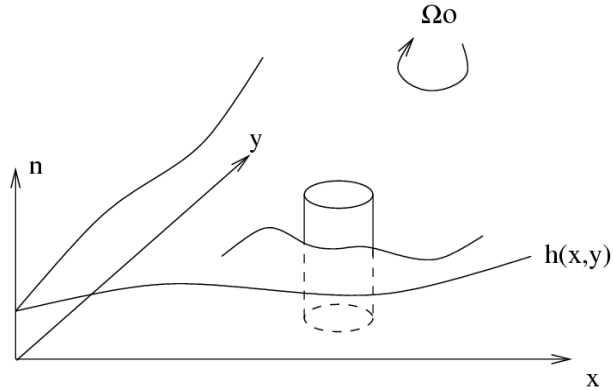


Figure 2. Shallow water model

We use the shallow water equations in a rotating frame which rotates clockwise to correspond to the Earth's rotation in the Southern hemisphere. These equations modelize the flow past an obstacle, taken here as a cylinder :

$$\frac{\partial \vec{V}}{\partial t} + (\vec{V} \cdot \nabla) \vec{V} + f \vec{n} \times \vec{V} + \nabla \phi = \nu \nabla^2 \vec{V}$$

$$\frac{\partial \phi}{\partial t} + \nabla \cdot (\phi \vec{V}) = 0$$

where $\vec{V}(x, y)$ is the velocity, $\phi(x, y) = gh(x, y)$ the geopotential with h the free surface height and g the Earth's gravity, $f = 2\Omega_0$ the coriolis parameter with Ω_0 the Earth's rotation, ν the kinematic viscosity and \vec{n} the normal to the plane (x, y) .

Taking the diameter D of the cylinder as the reference length scale and the velocity of the obstacle \vec{U} as the reference velocity scale, we consider the three adimensional parameters :

- the Reynolds number, which is the ratio of the advective and viscous terms, $Re = \frac{U D}{\nu}$,
- the Rossby number, which is the ratio of the advective and Coriolis terms, $Ro = \frac{U}{D \Omega_0}$,
- the Burger number, which is the ratio of the gravity and rotation effects, $Bu = \left(\frac{2R_d}{D}\right)^2$, where R_d is the deformation radius $R_d = \sqrt{\phi_0/f}$.

2.2 Numerical model

The shallow water equations are solved with a pseudo-spectral scheme for the space integration and a leapfrog scheme for the time integration (Farge and Sadourny 1989). The presence of the obstacle is imposed by using a volume penalisation method (Arquis and Caltagirone 1984; Kevlahan and Ghidaglia 2001; Schneider and Farge 2002), which considers both the fluid and the solid as the same porous medium, whose permeability tends to zero in the solid domain Ω_s , and to infinity in the fluid domain Ω_f . For this a Darcy's force term is added to the momentum equation, which is solved in the whole domain $\Omega = \Omega_s + \Omega_f$, considering periodic boundary conditions :

$$\vec{F} = -\frac{\chi}{\epsilon}(\vec{V} - \vec{U})$$

where $\epsilon \ll 1$ the penalization parameter and χ is the characteristic function of the obstacle such that :

$$\chi(\vec{x}) = \begin{cases} 1 & \text{for } \vec{x} \in \bar{\Omega}_s, \\ 0 & \text{for } \vec{x} \in \bar{\Omega}_f. \end{cases}$$

Therefore \vec{V} verifies the shallow water equations in Ω_f and is forced to \vec{U} in Ω_s . The effect of the penalized term is similar to having no-slip boundary conditions on the obstacle, which results in the formation of boundary layers and production of vorticity there. The penalized shallow water equations in the rotating frame are :

$$\frac{\partial \vec{V}}{\partial t} + (\vec{V} \cdot \nabla) \vec{V} + f \vec{n} \times \vec{V} + \nabla \phi = \nu \nabla^2 \vec{V} - \frac{\chi}{\epsilon}(\vec{V} - \vec{U})$$

$$\frac{\partial \phi}{\partial t} + \nabla \cdot (\phi \vec{V}) = 0$$

where \vec{U} is the velocity of the obstacle relative to the rotating frame. The initial conditions are $\vec{V}(t=0) = \vec{U}$ in the obstacle and zero elsewhere, and the free surface height is constant $\phi(t=0) = \phi_0 = 10^5 m^2 s^{-2}$, which gives a velocity of the gravity waves $c = \sqrt{\phi_0} = 316 m s^{-1}$.

The space discretization is $\Delta x = \frac{L_x}{1024} = \frac{\pi}{128}$ in the spanwise direction and $\Delta y = \frac{L_y}{256} = \frac{\pi}{128}$ in the streamwise direction with the domain length L_x, L_y such that $L_y = 2\pi$ and $L_x = 4L_y$. The time step is chosen to be smaller than the characteristic time of the fastest inertio-gravity waves $\Delta t = 0.25(1/\sqrt{(\frac{2\pi}{\Delta x})^2\phi_0 + f^2})$. The penalisation parameter is very small and such that $\epsilon = 2\Delta t$.

The convergence of the solutions of the penalized equations towards the solutions of the non-penalized equations has been proven for the Navier-Stokes equations (Angot et al. 1999), but not yet for the rotating shallow water equations. This is the reason why we have chosen to compare the numerical results with those of laboratory experiments, in order to validate the penalization method in this new context where both vortices and waves are dynamically important. The volume penalization presents the advantage of taking into account obstacles or complex geometries while keeping a Cartesian mesh and using a high-order pseudo-spectral scheme.

2.3 Laboratory model

The experiments are performed in a $48\text{ cm} \times 130\text{ cm}$ tank mounted on a 1.5 m diameter turn-table which is located at the Department of Mechanics (UME) of ENSTA, Palaiseau. The upper plate rotates clockwise, which corresponds to the rotation in the Southern hemisphere, and is supported by a thin air layer in order to reduce friction and avoid mechanical vibrations at the inertial frequency.

To satisfy the shallow water conditions the fluid is stratified with two layers: a thin upper layer of density ρ_1 and a thick lower layer of higher density $\rho_2 > \rho_1$ (cf. Figure 3). The difference of density between the upper layer and the air above enables us to neglect the deformation of the free surface compared to the deformation of the interface between the two layers. As the upper layer is thinner ($h = 2.5\text{ cm}$) than the bottom layer ($H = 20\text{ cm}$), the dynamics in the latter can be neglected in first approximation. To guaranty that horizontal scales dominate vertical scales, as required by the shallow water approximation, we use a cylinder whose diameter ($D = 7\text{ cm}$) is larger than the upper layer thickness. Since the cylinder is translated in the upper layer only, the resulting dynamics is similar to a rotating shallow flow with one free interface.

When the bottom layer has reached solid rotation, we slowly inject the upper layer. We wait until the upper layer attains solid rotation and we then impulsively translate the cylinder in the upper layer at velocity \vec{U} . Buoyant particles are added for visualization

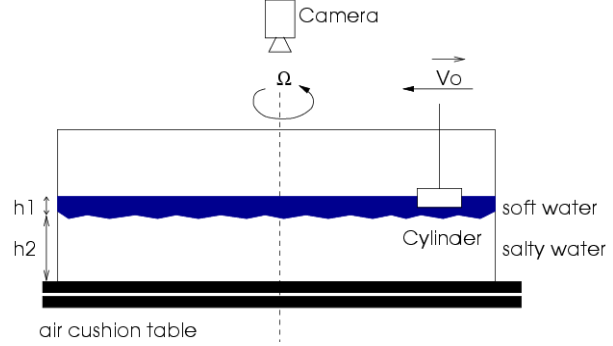


Figure 3. Laboratory experiment

tion and a CCD camera, fixed above the tank and rotating with it, captures the motion of particles which are lightened by a horizontal laser sheet. A standard PIV software is used to compute the velocity field and deduce the vorticity and the streamfunction fields.

3 RESULTS

3.1 Numerical results

In this paper we study the shallow water flow past an impulsively started cylinder in a rotating frame. We consider the following parameters : Reynolds number 400, Rossby number 0.24 and three different Burger numbers, 1, 0.25 and 0.1. In all cases the effect of rotation is significant since the radius of deformation is comparable or smaller to the cylinder radius. We compute the evolution of the following fields: vorticity $\omega = \nabla \times \vec{V}$, potential vorticity $(\omega + f)/\phi$, geopotential ϕ , stream function $\psi = \nabla^{-2}\omega$ and modulus of velocity $|\vec{V}|$. We integrate the shallow water equations during 30 periods of the rotating frame, $\tau_f = 2\pi/f = \pi/\Omega_0$.

We observe that during the flow evolution vorticity is produced in the boundary layers which is formed on the obstacle and a von Karman street develops in the wake. Both vorticity (Figure 4A) and potential vorticity (Figure 4B) exhibit an asymmetry of the wake : cyclones ($\omega > 0$) are elongated while anticyclones ($\omega < 0$) remain quasi-circular. This asymmetry is similar to what is observed in the Atlantic ocean in the wake of Isla Mujeres Island (cf. figure 1).

Figures 3C and 3D show that the flow is in geostrophic balance, since the surface height $h = \phi/g$ is similar to the stream function. Indeed, geostrophic balance is a stationary solution of the inviscid rotating shallow water equations in the limit of small Rossby numbers. For $Ro \ll 1$, the advective term is negligible compared to the Coriolis force and there is a balance between the gradient of geopotential and the Coriolis force :

$$f\vec{n} \times \vec{V} = -\nabla\phi$$

Velocity $V = \nabla \times \psi \vec{n}$, therefore $\nabla(f\psi + \phi) = 0$ and geostrophic balance gives therefore :

$$\psi = -\frac{\phi}{f} + cte$$

The modulus of velocity (Figure 4E) shows the formation of a background jet in the recirculation zone behind the cylinder. We also observe that the vortices are slowly damped by viscous dissipation and thus become more circular when they are far away down the wake.

The effect of rotation on the von Karman street is shown in Figure 5. As the Burger number decreases, *i.e.* the deformation radius becomes smaller than the radius of the cylinder, the cyclone-anticyclone asymmetry increases, *i.e.* cyclones become more elongated and deformed whereas anticyclones remain axisymmetric. We also observe that as the Burger number decreases the vortex shedding occurs further down in the wake and the distance between vortices decreases. Therefore the Strouhal frequency, which is the characteristic frequency of the vortex shedding for a flow past an obstacle, increases as the Burger number decreases.

3.2 Laboratory results

The horizontal extension of the laser sheet restricts the visualization window. Unlike the numerical experiment, the laboratory experiment does not allow to observe the whole wake at once. Taking into account this experimental restriction, we visualize the wake at two different locations. The first visualization (window A) is located just behind the cylinder (at 3 diameters distance), where the vortices are formed. While the second visualization (window B) is located further down the obstacle (at 8 diameters distance), where the vortex shedding occurs. We show here two experiments, which correspond to two sets of parameters: $Bu = 1$, $Ro = 0.25$, $Re = 371$ (Figure 6) and $Bu = 0.25$, $Ro = 0.31$, $Re = 1050$ (Figure 7). The main difference between these two sets of parameters is the Burger number, since we have observed that the change in Re is not significant in this case. We see that the size of the vortices formed just behind the cylinder depends on the Burger number (Figures 6A and 7A), because the deformation radius inhibits the spreading of the shear layer which is formed at the wall. Further down (Figures 6B and 7B) vortices increase in size, becoming larger than R_d , and anticyclones become axisymmetric while cyclones keep their elliptical shape for a long time.

Quantitative analysis of the velocity and the corresponding vorticity are obtained from PIV. According to Figure 8A the value of the local relative vorticity

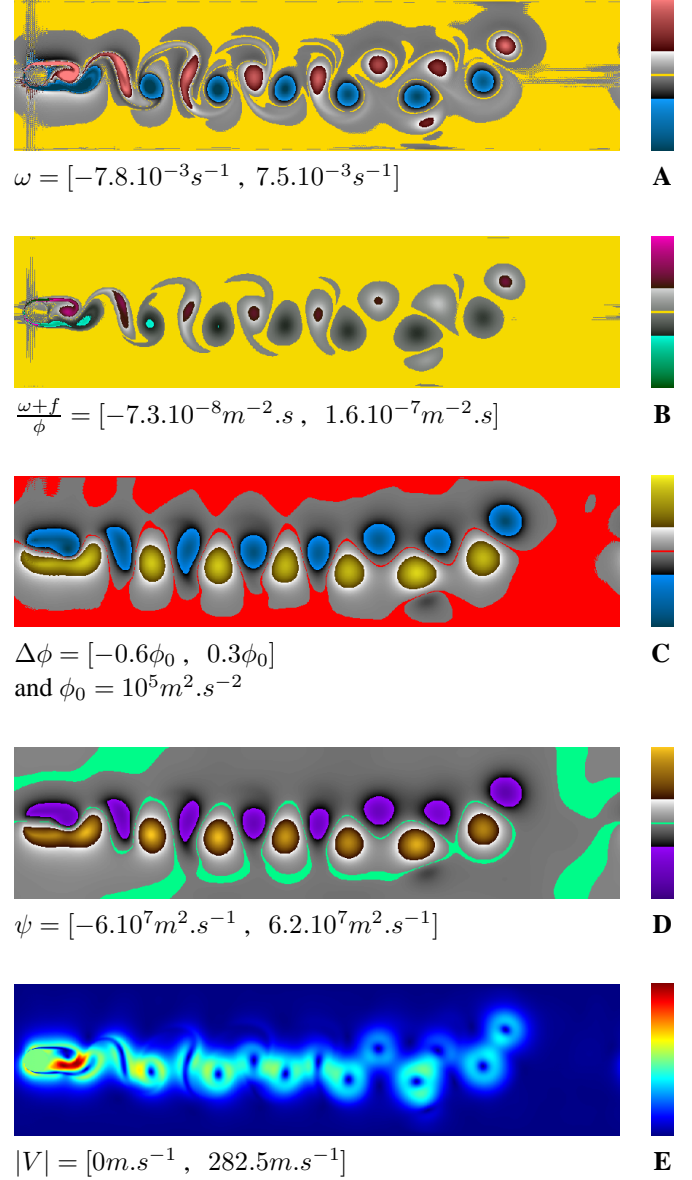
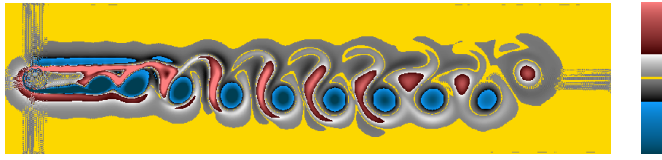


Figure 4. From top to bottom : vorticity, potential vorticity, geopotential, stream function and modulus of velocity fields at $t = 30 \tau_f$



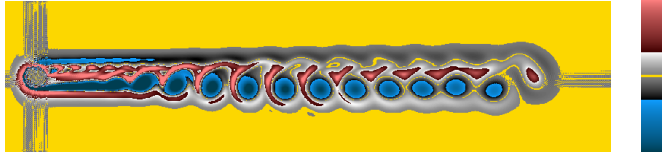
$$\omega = [-7.8 \cdot 10^{-3} s^{-1}, 7.5 \cdot 10^{-3} s^{-1}]$$

A



$$\omega = [-1.48 \cdot 10^{-2} s^{-1}, 9.8 \cdot 10^{-3} s^{-1}]$$

B



$$\omega = [-7.74 \cdot 10^{-2} s^{-1}, 6.95 \cdot 10^{-2} s^{-1}]$$

C

Figure 5. From top to bottom : vorticity fields at $Bu=1$, $Bu=0.25$, $Bu=0.1$ at $t=30 \tau_f$

ω/f measured during the formation of the vortices is roughly three times the Rossby number. Later on (Figure 8B) when the vortices are no more attached to the obstacle, the relative vorticity becomes twice the Rossby number. Hence, next to the obstacle where the shedding process occurs and downstream in the vortex street, the relative vorticity has a finite value ($\omega/f \simeq 0.5 - 0.8$), even if the Rossby number is small $Ro \simeq 0.25 - 0.31$.

3.3 Interpretation

The cyclone-anticyclone asymmetry (elongated cyclones compared to quasi-circular anticyclones) observed both in numerical and laboratory experiments is not yet fully understood. However, according to previous works (Polvani et al. 1994; Stegner and Dritschel 2000; Poulin and Flierl 2003), this asymmetry occurs when the relative deviation of the free surface $\lambda = \Delta h/h$ becomes non negligible.

In rotating shallow water flows, the slow component of motion (*i.e.* the vortical motion but not the wave motion) satisfies, at the leading order, the geostrophic balance. Therefore the relative deviation of the free surface λ scales as Ro/Bu . Hence, both large scale-effects, namely small Burger number, and finite Rossby number tend to increase the free surface deformation. In a regime where λ becomes large, cyclonic and anticyclonic structures will not have the same dynamical behaviour. Indeed, anticyclones can locally satisfy $\lambda \geq 1$ while cyclones are bounded by $\lambda = -1$. Hence, this condition restricts the size of the cyclones satisfying the geostrophic balance and lead to their elongation.

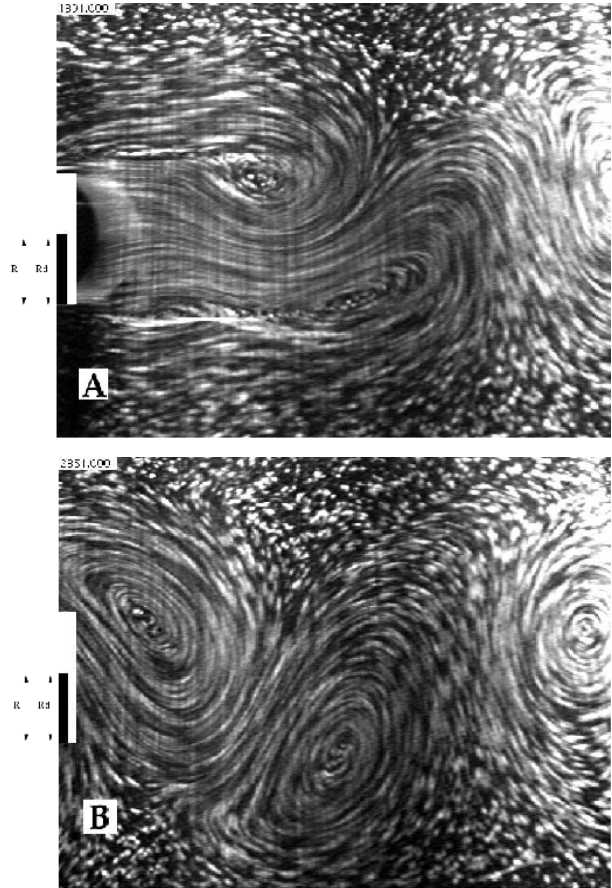


Figure 6. Visualization of particles motion just behind the cylinder, at $t = 0$ (A), and at $t = 4\tau_f$ (B), for $Re \simeq 400$, $Bu \simeq 1$, $Ro \simeq 0.25$. The white (black) marker indicates the cylinder diameter D (deformation radius R_d).

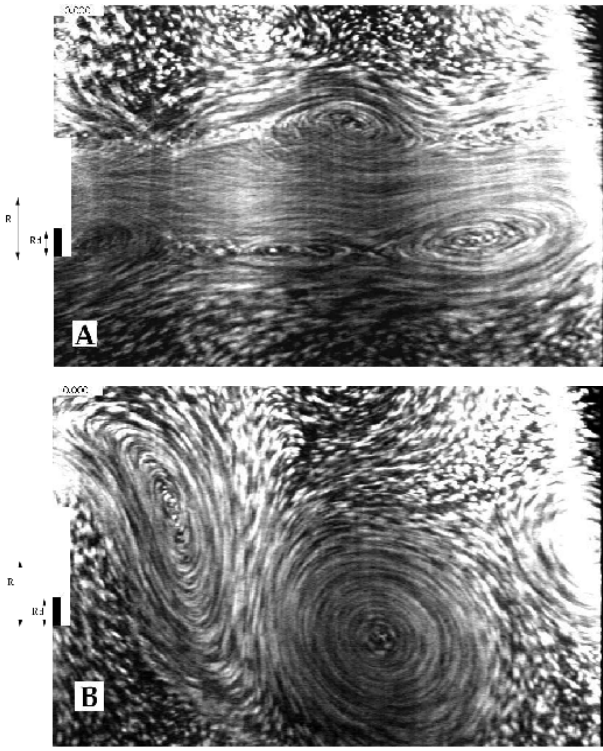


Figure 7. Visualization of the particles trajectories (streaklines) just behind the cylinder, at $t = 0$ (A), and at $t = 4\tau_f$ (B), for $Re \simeq 1050$, $Bu \simeq 0.25$, $Ro \simeq 0.3$. The white marker on the left corresponds to the cylinder radius R , and the black marker indicates the deformation radius R_d .

According to the numerical simulations (Figure 4), the vorticity of detached cyclones and anticyclones have roughly the same amplitude, while the free surface deviation is stronger for cyclones. This is due to the centrifugal force which is no more negligible compared to the Coriolis force when the relative vorticity has a finite value. In such case, the centrifugal terms induce a depression in the core of vortical structures of both signs. Hence, this cyclostrophic effect added to the geostrophic balance reduces (increases) the free surface elevation (depression) of anticyclones (cyclones).

4 CONCLUSION

We have performed both numerical and laboratory experiments, for Burger numbers equal to 1 and 0.25. Although in the laboratory experiments the Reynolds number differs significantly for both cases, we assume that rotation effects dominate inertial effects in the regime considered here and therefore the variation of the Reynolds number does not affect the results. We have found that the von Karman street formed in the wake presents an asymmetry between cyclones and anticyclones. Both numerical and laboratory experiments qualitatively agree on this and show that this asymmetry increases when the Burger number decreases, *i.e.* the effect of rotation increases. These results are preliminary and in further work we will perform more quantitative comparisons. We also plan to compute the lift and drag, and study the production of vorticity in the boundary layers which develop on the obstacle.

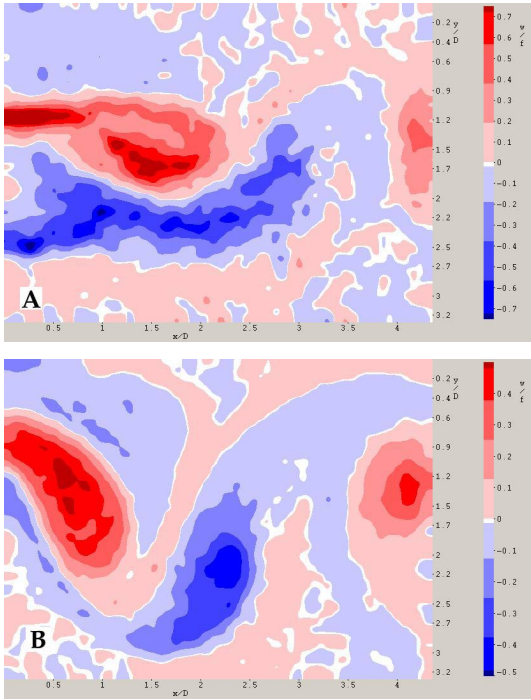


Figure 8. Vorticity field for $Re \simeq 400$, $Bu \simeq 1$, $Ro \simeq 0.25$ at $t = 9.3\tau_f$ (A) and $t = 12\tau_f$ (B).

REFERENCES

- Angot, P., C.-H. Bruneau, and P. Fabrie (1999). A penalization method to take into account obstacles in viscous flows. *Num. Math.* 81, 497–520.
- Arquis, E. and J. P. Caltagirone (1984). Sur les conditions hydrodynamiques au voisinage d'une interface milieu fluide-milieu poreux : application à la convection naturelle. *C. R. Acad. Sci. Paris II* 299, 1–4.
- Farge, M. and R. Sadourny (1989). Wave-vortex dynamics in rotating shallow water. *J. Fluid Mech.* 206, 433–462.
- Kevlahan, N. and J.-M. Ghidaglia (2001). Computation of turbulent flow past an array of cylinders using a spectral method with brickman penalization. *Eur. J. Mech.* 20, 333–350.
- Polvani, L. M., J. C. McWilliams, M. A. Spall, and R. Ford (1994). The coherent structures of shallow-water turbulence : deformation-radius effects, cyclone/anticyclone asymetry and gravity-wave generation. *Chaos* 4(2), 177–186.
- Poulin, F. J. and G. R. Flierl (2003). The nonlinear evolution of barotropically unstable jets. *Journal of Physical Oceanography in press*.
- Schneider, K. and M. Farge (2002). Adaptive simulation of a flow around an impulsively started cylinder using penalization. *Appl. Comput. Harm. Anal.* 12, 374–380.
- Stegner, A. and D. G. Dritschel (2000). A numerical investigation of the stability of isolated shallow water vortices. *Journal of Physical Oceanography* 30, 2562–2573.